ARMY RESEARCH LABORATORY

Exploring the Ability of a Coarse-grained Potential to Describe the Stress-strain Response of Glassy Polystyrene

by Thomas W. Rosch, John K. Brennan, Sergey Izvekov, and Jan W. Andzelm

ARL-TR-6222 **October 2012**

NOTICES

Disclaimers

The findings in this report are not to be construed as an official Department of the Army position unless so designated by other authorized documents.

Citation of manufacturer's or trade names does not constitute an official endorsement or approval of the use thereof.

Destroy this report when it is no longer needed. Do not return it to the originator.

Army Research Laboratory
Aberdeen Proving Ground, MD 21005

ARL-TR-6222 **October 2012**

Exploring the Ability of a Coarse-grained Potential to Describe the Stress-strain Response of Glassy Polystyrene

Thomas W. Rosch
Oak Ridge Institute for Science and Education

John K. Brennan, Sergey Izvekov, and Jan W. Andzelm
Weapons and Materials Research Directorate, ARL

REPORT DOCUMENTATION PAGE

Form Approved
OMB No. 0704-0188

1. REPORT DATE *(DD-MM-YYYY)*	2. REPORT TYPE	3. DATES COVERED (From - To)
October 2012	Final	1 January 2012 to 30 June 2012

4. TITLE AND SUBTITLE
Exploring the Ability of a Coarse-grained Potential to Describe the Stress-strain Response of Glassy Polystyrene

5a. CONTRACT NUMBER

5b. GRANT NUMBER

5c. PROGRAM ELEMENT NUMBER

6. AUTHOR(S)
Thomas W. Rosch, John K. Brennan, Sergey Izvekov, and Jan W. Andzelm

5d. PROJECT NUMBER

5e. TASK NUMBER

5f. WORK UNIT NUMBER

7. PERFORMING ORGANIZATION NAME(S) AND ADDRESS(ES)
U.S. Army Research Laboratory
ATTN: RDRL-WMM-G
Aberdeen Proving Ground, MD 21005

8. PERFORMING ORGANIZATION REPORT NUMBER
ARL-TR-6222

9. SPONSORING/MONITORING AGENCY NAME(S) AND ADDRESS(ES)

10. SPONSOR/MONITOR'S ACRONYM(S)

11. SPONSOR/MONITOR'S REPORT NUMBER(S)

12. DISTRIBUTION/AVAILABILITY STATEMENT
Approved for public release; distribution unlimited.

13. SUPPLEMENTARY NOTES

14. ABSTRACT

Molecular dynamics simulations were performed to calculate the stress-strain behavior of a coarse-grained (CG) potential corresponding to polystyrene. The force-matching (FM) technique was used to calculate the nonbonded interactions at a CG resolution of one CG site per monomer. The Inverse Boltzmann Inversion (IBI) method was used to parameterize the bonded and bond angle bending interactions. The CG model exhibited a significantly lower modulus compared to the atomistic model at low temperature and high strain rate. Addition of friction through use of the constant-temperature dissipative particle dynamics (DPD) method improved the modulus, yet was not transferrable to higher temperatures and lower strain-rates. An increase of attraction between CG beads by direct manipulation of the nonbonded potential also improved the stress response. Two parameterization protocols that shifted the force to more attractive values were explored. One corresponded to a uniform shift and the other shifted the force in a more localized region. The uniformly shifted potential greatly affected the structure of the equilibrium model as compared to the locally shifted potential, yet was more transferrable to different temperatures and strain-rates.

15. SUBJECT TERMS
Force-match, polystyrene, coarse-grain, deformation

16. SECURITY CLASSIFICATION OF:			17. LIMITATION OF ABSTRACT	18. NUMBER OF PAGES	19a. NAME OF RESPONSIBLE PERSON
a. REPORT	b. ABSTRACT	c. THIS PAGE			Thomas W. Rosch
Unclassified	Unclassified	Unclassified	UU	36	19b. TELEPHONE NUMBER (*Include area code*) (410) 306-1926

Contents

List of Figures

INTENTIONALLY LEFT BLANK.

1. Introduction

Coarse-grained (CG) potentials have the ability to extend the length and time scale that can be examined using simulation. By grouping atoms together into effective interaction sites, it is possible to examine phenomena and calculate macroscopic properties inaccessible from purely fine resolution considerations. Calculations of mechanical properties in polymer systems are particularly suited for this treatment because of the range of length and time scales that describe all the relevant physics within. For example, polymer bonded properties are of the order of 0.1 nm, yet chains in entangled polymer systems may span 10–100 nm, both of which affect mechanical properties.

One approach to investigate mechanical properties of polymer systems has been to use a simple generic model that incorporates the most pertinent interactions within and between atoms. In this model, monomers or even groups of monomers are modeled as beads that are connected to adjacent beads by a finitely extensible nonlinear elastic (FENE) potential. Non-adjacent beads interact with a shifted Lennard-Jones potential. This potential was developed by Kremer and Grest (*1*) and used to simulate strain hardening phenomena (*2*) and glass transition (*3*) of linear polymers. The FENE potential has since been modified slightly to allow for bond breaking and has been employed by many researchers to investigate a variety of polymer deformation phenomena. For example, Tsige and Stevens studied adhesion failure in highly crosslinked polymers (*4*). Rottler et al. (*5*) and Panico et al. (*6*) applied tension on systems with slightly different bonded potentials to study failure in glassy linear polymers at moderate and large strains, respectively. Mukherji and Abrams also used a modified FENE potential to examine microvoid formation and strain hardening in cross-linked polymers (*7*). Bulacu and van der Giessen have changed polymer chain stiffness by including 3- and 4-body terms between beads and studied its effect on the glass transition (*8*). Riggleman and coworkers applied a similar model to examine mobility during creep of both a linear polymer and nanocomposite, where adjacent beads were connected with stiff harmonic bonds instead of the FENE potential (*9*). Although such studies have been able to greatly advance our understanding of the link between microscopic interactions and macroscopic polymer deformation phenomena, they lack the ability to describe chemically specific systems.

Many recipes exist to develop a CG potential to model a specific system of interest. In general, chemical information can incorporated from atomistic or near-atomistic resolution simulations at a given state point to provide reference data. The desired level of CG is applied to this reference data and parameterization is obtained by matching certain properties between the two levels of resolution. One procedure that deterministically obtains CG potential parameters is called iterative Boltzmann inversion (IBI), which Reith and coworkers applied to parameterize a CG potential for polyisoprene (*10*). IBI sequentially decreases the difference between the free

energies of the CG and atomistic distribution functions. To obtain parameters for bonded interactions, one applies the IBI procedure using bond, angle, or dihedral probability distributions, while for nonbonded interactions the radial distribution function is used. Müller-Plathe successfully parameterized a CG potential for polystyrene at a resolution of one CG bead per monomer using IBI and examined the ability of the potential to describe equilibrium properties at other temperatures (*11*).

Another method to obtain CG potentials for polymer systems has been used by Fritz and coworkers (*12*). Unlike the studies mentioned previously, atomistic simulations were not performed in the melt. The authors instead ran a constraint dynamics simulation on two trimers in vacuum and calculated the pair potential of mean force along the distance coordinate. The potential of mean force can then be integrated to determine the pair potential between CG beads. Analogously, the bonded CG potential is calculated by obtaining bond and angle distributions for a single long chain in vacuum. Surprisingly, the calculated potential was able to reproduce densities and structural distributions in the melt over a range of temperatures. Guerrault and coworker applied a similar method to calculate a CG forcefield for polyethylene (*13*), yet potentials of mean force were calculated in a melt state from reference Isothermal-Isobaric (NPT) Monte Carlo simulations. This CG forcefield was then used to calculate equilibrium properties across a range of chain lengths.

Using the IBI approach or the potential of mean force to parameterize a CG potential by definition captures two body correlations, yet may have severe limited state-point transferability (*14*). State-point transferability refers to the ability of a CG potential to describe a given property correctly at another state-point (i.e., temperature, density, pressure) than the one used in the parameterization scheme. Also of importance is *observable transferability*, which refers to the ability of a CG potential to correctly describe an observable that has not been used in its parameterization. In addition to limited transferability, structure-based approaches assume that there is a unique mapping of pair correlations onto pairwise potentials. The validity of this assumption is not readily apparent for complex systems. A direct method to obtain force field parameters introduced by Izvekov et al. (*15*) addresses the above problems. The approach equates the multi-body force acting upon a CG bead to that of the atomistically detailed reference system. This bottom-up multiscale coarse-graining (MS-CG) method has been successfully applied to ionic liquids (*16*), small peptides (*17*), and molecular crystals (*18*).

While the MS-CG method improves transferability by incorporating multi-body effects, no CG method is able to accurately reproduce every property of the atomistic ensemble. Depending upon the phenomena of interest that one needs to capture using the CG potential, improvement can be achieved by including additional information from the atomistic simulations. For instance, CG potentials parameterized using IBI often result in pressure or density differences between the CG and atomistic system. A common practice is to shift the CG potential to more attractive values until pressures or densities match. Improved performance in equations of state

calculations using MS-CG has been realized by aggregating density dependent potentials to investigate properties at vastly different state-points (*18*, *19*).

While the above methods to incorporate chemical specificity have been applied to calculate static properties, they have been used very infrequently to study mechanical properties. Pioneering work conducted by Lyulin and coworkers (*20*) investigated the microscopic origins of strain-hardening in polystyrene and polycarbonate. A united atom model, where the hydrogen and carbon atoms are coarse-grained into a single-site representation, was used. While the united atom model is a very low level of coarse-graining, computational requirements were reduced and Lyulin and coworkers were able to demonstrate that non-affine mobility upon deformation is linked to strain-hardening effects.

Finally, a recent paper by Majumder et al. (*21*) investigated the ability of extending the coarse-graining of polystyrene further and using a coarser potential to calculate mechanical properties. Like Lyulin and coworkers, the authors used united atom simulations as reference data upon which the force-matching (FM) technique of Izvekov et al. was applied to determine a CG potential that represented each polystyrene monomer by one CG bead. The FM technique was shown to give a potential that greatly overestimated the pressure. Consequently, Majumder and coworkers modified the potential to fit a Lennard-Jones type interaction and adjusted the parameters to match the pressure between the CG and united atom simulations. This procedure was shown to reproduce the glassy stress-strain curve at high deformation rate.

In this work, we further examine the ability of chemically informed CG potentials to describe mechanical properties. Molecular dynamics simulations of amorphous polymers for an all-atom resolution governed by the PCFF forcefield (*22*) served as reference data. The FM procedure of Izvekov et al. was performed at a resolution of one CG bead per monomer. In order to more closely match the structure between the CG and atomistic resolution, the iterative Boltzmann inversion method was used to determine the CG bonded potentials. Stress-strain extension simulations were then performed and the viability of the CG potentials assessed.

2. Methodology and Simulation Details

Molecular dynamics simulations were performed using the open-source code Large-scale Atomic/Molecular Massively Parallel Simulator (LAMMPS) (http://lammps.sandia.gov) (*23*). The commercial visualization package Materials Processes and Simulations (MAPS) (http://www.scienomics.com) was used to create a periodic cell and assign the PCFF forcefield (*22*). Partial charges located on the atomic sites were governed by the Condensed-phase Optimized Molecular Potentials for Atomic Simulation Studies (COMPASS) forcefield, which were obtained using Materials Studio. Although COMPASS is an improvement upon the PCFF forcefield, many of the parameters are proprietary and cannot be ported to the LAMMPS

simulation code. In our molecular dynamics simulations at the atomistic resolution, we used a cutoff of 12.0 Å for both Lennard-Jones (van der Waals) and Coulombic nonbonded interactions. Long-range electrostatic interactions were calculated using the particle-particle particle-mesh method with a precision of 1.0e-6. Temperature was maintained by a Nose-Hoover thermostat with a coupling constant of 100 fs. For NPT simulations, the pressure was controlled by a Nose-Hoover barostat with a coupling constant of 1000 fs. Simulations at the atomistic resolution used a timestep of 1 fs, while CG simulations used a timestep of 2 fs.

This study focuses on one level of CG, namely one CG site per monomer. To begin, an atomistic trajectory in both the glassy (298.15 K) and rubbery (500 K) state were generated. At the outset of the work, it was unclear which state-point would produce reference information that will best transfer to other state-points. One might think that the information obtained in the glassy state would better describe the physics necessary to obtain stress-strain curves at other glassy states. Conversely, an atomistic trajectory generated at 500 K would explore more phase space that might produce a more transferrable forcefield. To insure equilibrated structures at the beginning of the glassy atomistic trajectory, initial amorphous systems are relaxed and annealed. Relaxation consists first of energy minimization using the Polak-Ribiere conjugate gradient with a maximum of 10000 steps, and energy and force tolerance of 0 and 1.0e-8, respectively. After minimization, four consecutive microcanonical ensemble (NVE) simulations of 10000 steps were performed with timesteps of 0.001, 0.01, 0.1, and 1 fs, respectively. Annealing the structure consisted of five cycles of an NPT simulation. Each cycle contained 50 ps at 298.15 K, heating to 600 K at a rate of 0.67 ps/K, 50 ps at 600 K, cooling to 298.15 K at a rate of 0.1656 ps/K, and finally an energy minimization. After the annealing process, the structure was subjected to 10 ns of NPT simulation under ambient conditions, where atomic positions, forces, and velocities were recorded every 1 ps. The rubbery trajectory started from an equilibrated glassy system, which was heated to 500 K at a rate of 5ps/K and then 3 ns in the NPT ensemble were run, where positions, forces, and velocities were recorded every 1 ps.

A CG trajectory is mapped onto the last 3 ns (3000 snapshots) of a trajectory by applying the following equations:

$$R_I = \sum_{i=1,s} c_{Ii} r_i \,, \tag{1}$$

$$\sum_i c_{Ii} = 1 \,, \tag{2}$$

where R_I is the position of CG site I, r_i is the position of atom i, and s is the number of atoms in one CG site. $c_{Ii} = m_i/M_I$, where m_i is the mass of atom i and M_I is the mass of CG site I. At each snapshot, the atomic forces and velocities were coarse-grained following an analogous equation.

$$F_I = \sum_{i=1,s} f_i$$
$$V_I = \sum_{i=1,s} v_i \qquad (3)$$

Using a small subset of the overall trajectory (10 of the 3000 snapshots), the CG forces as a function of distance were calculated as a result of matching to the atomistic data following the procedure of Izvekov et al. (*24*). The resulting 300 functions for the overall trajectory were then averaged together to give the final tabulated CG force.

Initially, it was unclear how large the system needed to be to ensure that the properties calculated did not suffer from system size effects. For polystyrene, a large system consisting of 13 chains of 170 monomers (~35,000 atoms) and a small system consisting of 7 chains of 20 monomers (~2200 atoms) were generated. The nonbonded potential resulting from the force matching procedure between beads for the CG resolution of one site per monomer for each system size is shown in figure 1. The close match between both curves suggests that parameterization of the forcefield can be done on a relatively small system, which saves computational expense. Figure 2 displays the CG force profile obtained from the glassy and rubbery trajectory for a small system size. Perhaps surprisingly, application of the FM technique on trajectories generated at two very different temperatures does not produce large differences in the potential. The largest difference arises in smaller separations, where the curve parameterized at higher temperature corresponds to more repulsive values. The curve parameterized at 500 K also contains a slightly deeper well. Following the procedure of Izvekov et al., we used the 500 K curve for the rest of this work because the higher temperature allows for greater sampling of phase space, which should allow for greater transferability.

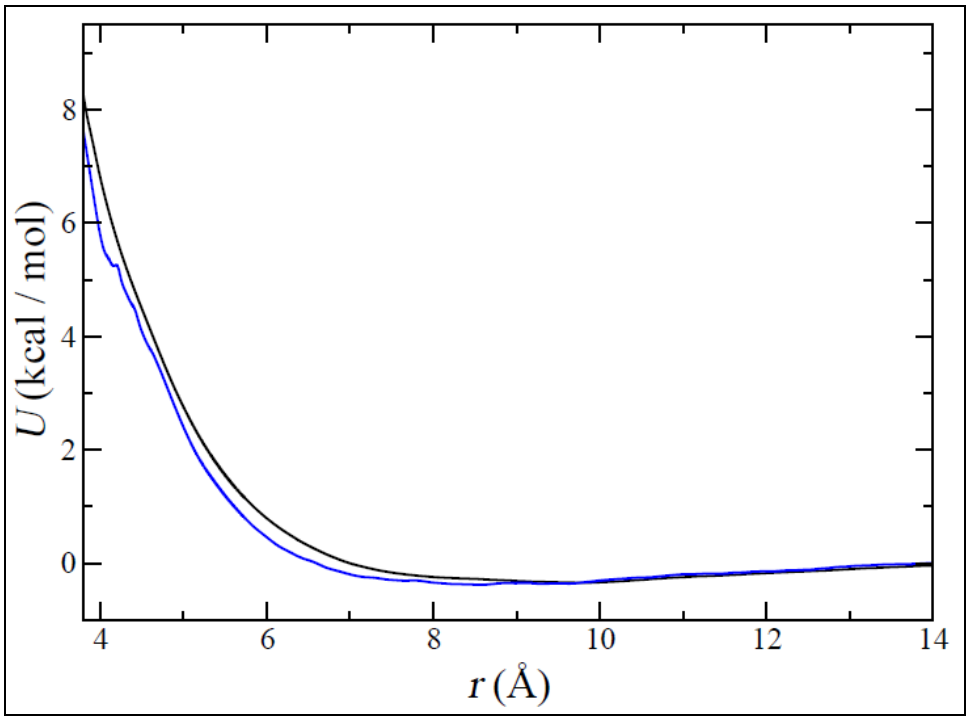

Figure 1. Nonbonded potential between CG beads of polystyrene parameterized at 100 K. Black and blue curves correspond to results of FM procedure on 35,000- and 2200-atom systems, respectively.

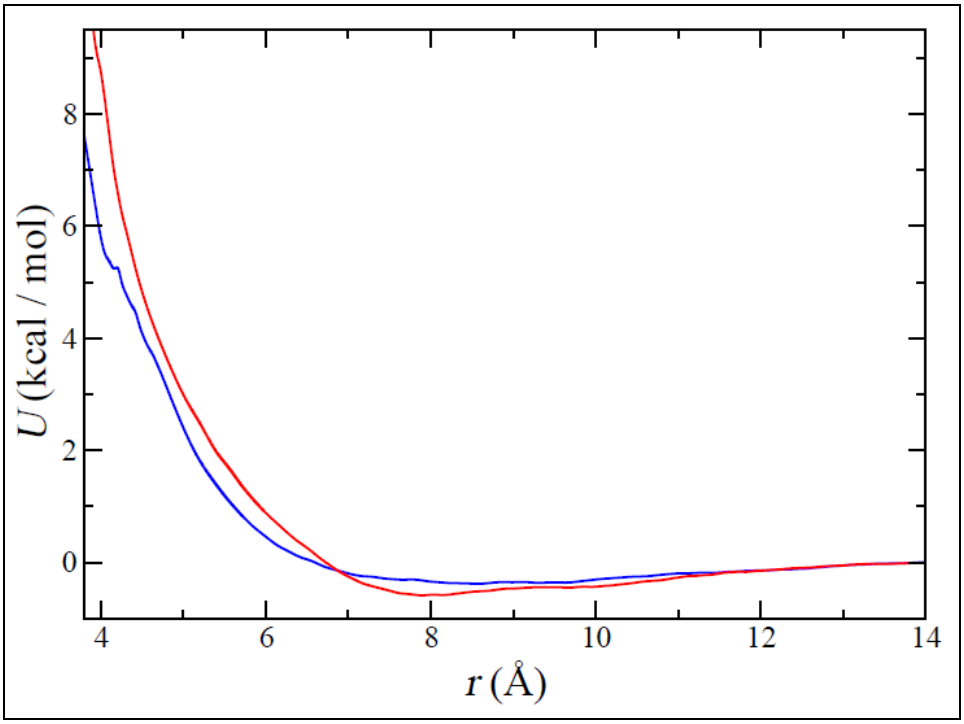

Figure 2. Nonbonded potential between CG beads of polystyrene parameterized at two different temperatures. Blue and red curves correspond to parameterization at 298 and 500 K, respectively.

3. Results and Discussion

To verify the CG potentials calculated through the FM procedure at 500 K, bond, angle, and radial distribution functions of the CG system were calculated. The CG system was generated from the last configuration of the large atomistic system (~35,000 atoms resulting in 2210 CG sites), and distribution functions were calculated from a 3-ns NVT simulation with a time step of 2 fs at the average atomistic density of 0.88 g/cm^3. Figure 3a–c displays the bond, angle, and radial distribution functions. The bonded and radial distributions match reasonably well for the atomistic and CG resolutions, while angular distributions are markedly different. Current implementation of the FM technique is purely radial-based, which does not allow for a direct calculation of angular potentials; thus, while 1–3 interactions were of the correct distance, their orientation does not match the atomistic distributions. In addition, the potentials calculated exclusively using the FM technique result in a density of 0.78 g/cm^3, an 11% difference.

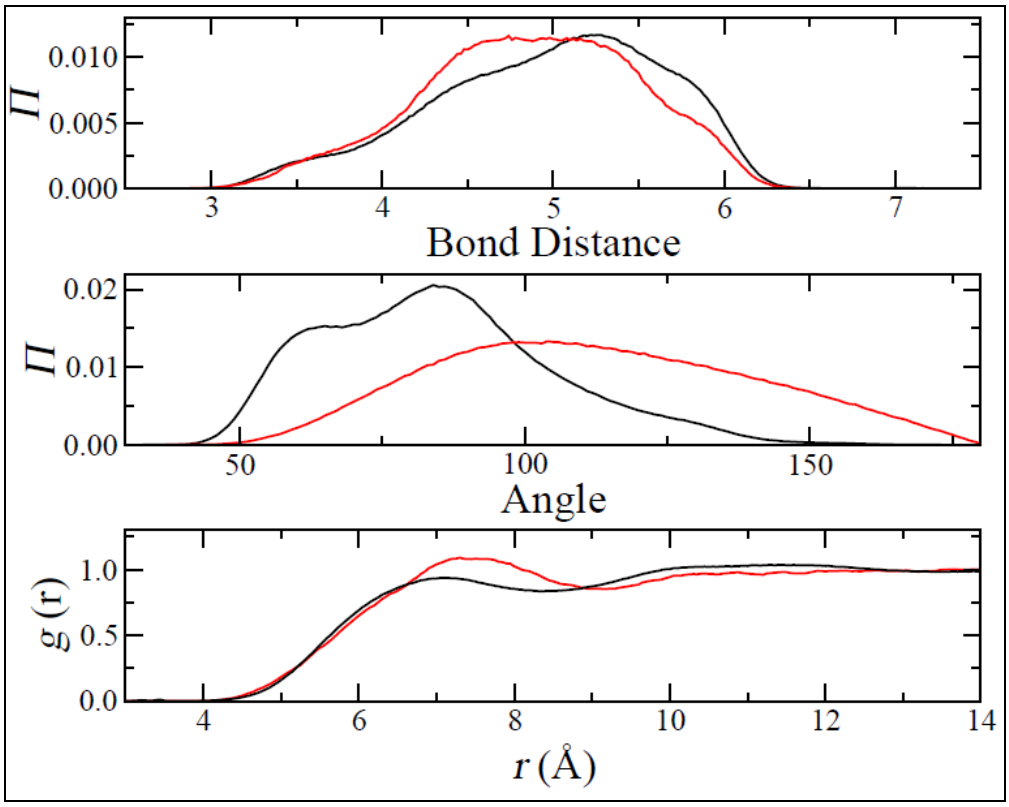

Figure 3. Distribution functions of the atomistic (black) and CG (red) models. (a), (b), and (c) are the bond, angle, and radial distribution functions. Both bonded and nonbonded potentials are determined from a FM protocol.

To improve upon the internal structure of the CG polymer chains, the iterative Boltzmann inversion method was applied to calculate both bond and angle potentials. An initial guess of the

potentials was based upon the probability distributions shown in figure 3a and b (black curves) as follows:

$$U_i = -k_B T \ln \Pi_i \,, \tag{4}$$

where *i* is the bond distance or angle of the distribution. A 2-ns simulation in the NVT ensemble (at the average density from the atomistic trajectory) was then run. An improved potential was then calculated from the difference of the new distributions and the target distributions:

$$U_{i,new} = U_{i,current} + \ln\left(\frac{\Pi_{i,current}}{\Pi_{i,target}}\right). \tag{5}$$

The progression of the bond distribution upon the IBI procedure is shown in figure 4. Convergence upon the target distribution is efficient, and the CG bond distribution lies on top of the distribution calculated from the atomistic distribution after three iterations. Similar results were seen for the angular distribution, which along with the bond and radial distribution functions, are shown in figure 5a–c. The blend of IBI (for bonded interactions) and FM (for nonbonded interactions) produces CG distributions that accurately reproduce the atomistic structure. It should be noted that the nonbonded interactions between CG beads containing the IBI bonded interactions in figure 2 is shifted to more attractive values so that the CG virial is 5% lower than the atomistic virial. This shift corrects the density discrepancy, resulting in CG values that are within 3% of the atomistic density.

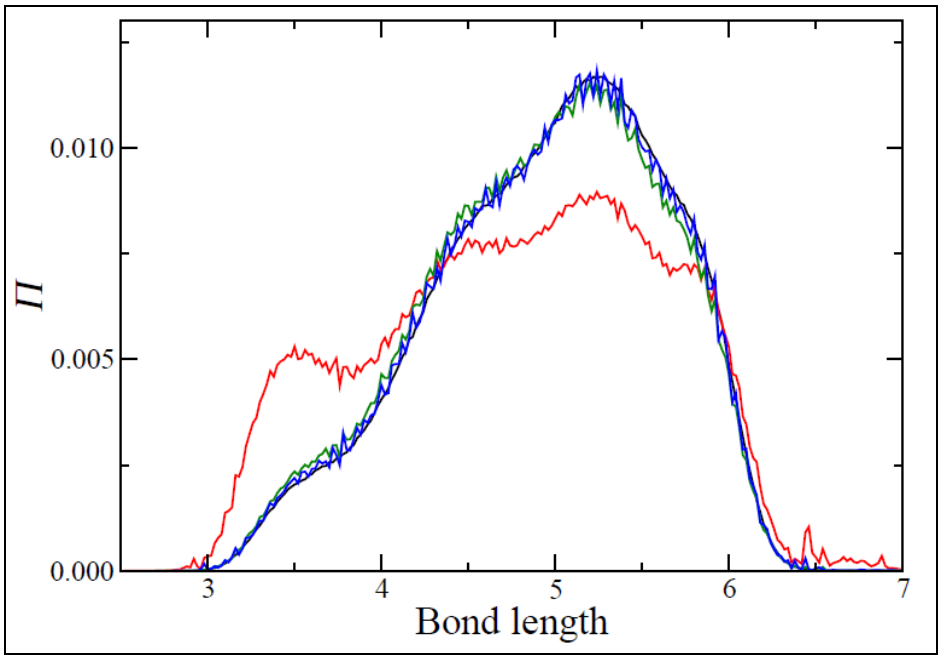

Figure 4. Bond probability distribution for different iterations. Red, green, blue correspond to iteration 1, 2, and 3, respectively.

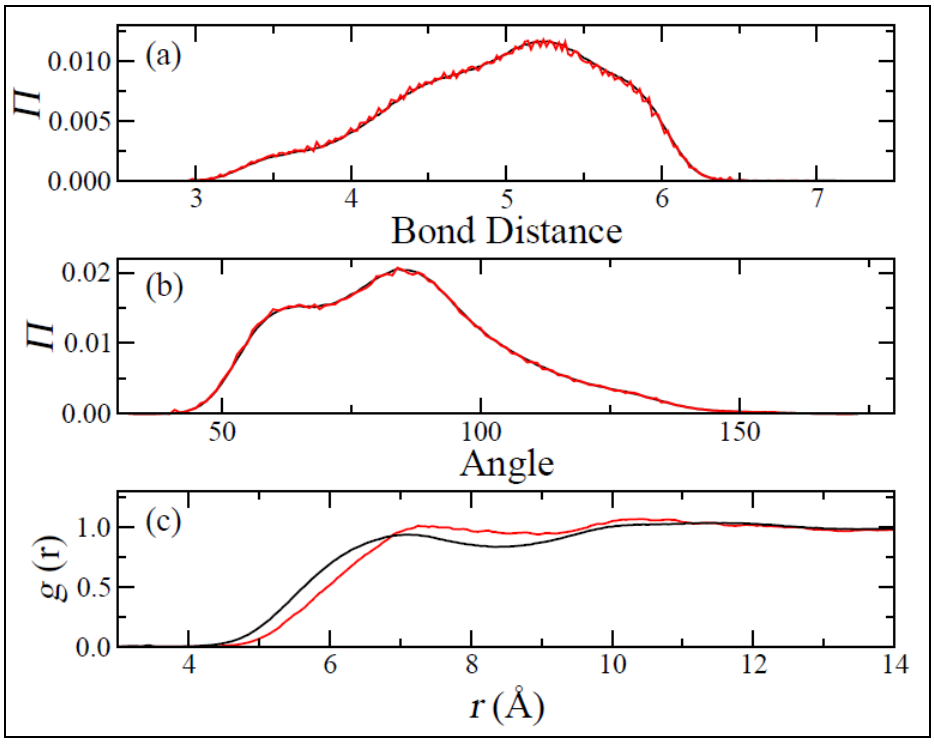

Figure 5. Distribution functions of the atomistic (black) and CG (red) models. (a), (b), and (c) are the bond, angle, and radial distribution functions. Bonded and angular potentials are determined using iterative Boltzmann inversion. The nonbonded potential is determined from FM protocol (same potential as in figure 2).

The potentials that produced the distributions in figure 5 were then used to examine the CG system's stress-strain behavior in a glassy state. We first examined the stress response at 100 K and a strain rate of 5e9 s^{-1} since these conditions were also examined by Majumder et al. (*21*). While this seems like an excessively low temperature, this ensures that the CG system is indeed a glassy state. The high strain rate should not have any qualitative effect on the stress behavior except to shift the yield to higher values. Also, the purpose of this study was not to compare to experiment, but to examine how well one can describe stress-strain behavior using CG potentials. To generate a curve for the atomistic system, five independent systems were constructed. These 5 independent systems of 13 polymers comprised of 170 monomers were equilibrated at 500 K, quenched to 100 K at a rate of 1 ps/K, and then strained at a rate of 5e9 s^{-1} in the x-, y-, and z-directions. Following the protocol of Vorselaars and cowokers (*25*), we report the stress as the von Mises equivalent:

$$\sigma_{vM} = \sqrt{\frac{1}{2}\left(\sigma_x - \sigma_y\right)^2 + \frac{1}{2}\left(\sigma_y - \sigma_z\right)^2 + \frac{1}{2}\left(\sigma_z - \sigma_x\right)^2} \quad . \tag{6}$$

Every data point is the average of the measured stress between each subsequent data point. In addition, for the atomistic system, the data point is the average of each 15 independent runs. The atomistic stress-strain curve displayed in figure 6 has two distinct regimes, the elastic at small strains and inelastic at large strains. The yield point for the atomistic system at this temperature and strain is ~310 MPa corresponding to ~10% strain with a small softening area corresponding to ~30% strain, and finally a strain hardening regime. While this yield point is very high, stress-strain simulations were also run at the conditions of Vorselaars and coworkers (*25*) study (temperature of 298 K and strain rate of 1e8 s^{-1}), and it was found that our system's mechanical properties matched very well with theirs. While this validates the method under which we calculate the stress-strain curves, the object of this study is to determine how well a CG potential can describe atomistic mechanical properties. The middle curve in figure 6 corresponds to the CG system with bonded potentials parameterized with IBI and nonbonded potentials parameterized with FM, shifted slightly to reproduce the correct density. As evident, there is no discernible yield point, along with a substantially smaller elastic and strain hardening modulus. The bottom curve corresponds to the CG system with both bonded and nonbonded potentials parameterized with FM. It should be noted that the CG strain-curves were generated with only one replica, yet adding the statistics from running on the extra replicas would not significantly change the overall behavior of the stress-strain curve. A larger CG system (160 polymers comprised of 100 monomers) was also simulated to ensure there are no system size effects. The results from both CG systems were statistically equivalent.

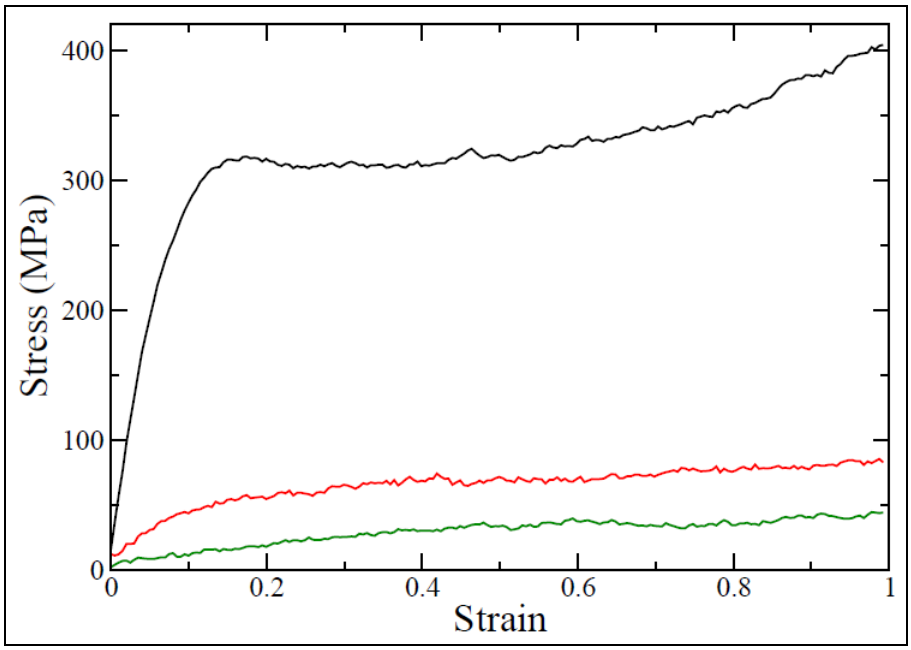

Figure 6. Stress-strain curves at 100 K and a strain rate of 5e9 s^{-1}. The top curve corresponds to the fully atomistic system (35,000 atoms). The middle and bottom curve correspond to CG systems with IBI+FM and FM-only potentials, respectively. The CG systems are the same absolute sizes as the atomistic system (2200 CG sites).

It is apparent from figure 6 that the pertinent physics is missing from the CG system to accurately describe stress-strain behavior found in the atomistic system. It is well known that CG potentials result in faster diffusion times of CG particles as compared to atomistic counterparts because they are smoother and softer (*26*). One way of controlling the diffusion of particles in a simulation is to run with a dissipative particle dynamics (DPD) thermostat. In addition to the force arising from dispersion and/or electrostatic interactions, the DPD thermostat includes dissipative and random forces. The arithmetic forms of these two forces are given below:

$$F_{ij}^{D} = -\gamma\left(1-\frac{r_{ij}}{r_c}\right)^2\left(\hat{\mathbf{r}}_{ij}\cdot\mathbf{v}_{ij}\right)\hat{\mathbf{r}}_{ij}$$
$$F_{ij}^{R} = \frac{\sigma\theta_{ij}}{\sqrt{\delta t}}\left(1-\frac{r_{ij}}{r_c}\right)\hat{\mathbf{r}}_{ij} \qquad (7)$$

where γ, σ, θ_{ij}, and δt are the dissipative scaling factor, noise level, random number, and timestep, respectively. Espanol and Warren derived the required fluctuation-dissipation relation between the dissipative scaling factor and noise level to sample from the canonical ensemble (*27*). By setting the dissipative term, one can effectively slow down the system dynamics, and in terms of CG systems, match the dynamics of the atomistic system.

In a glassy system it is very difficult to measure diffusion because it is exceedingly small. We therefore measured the diffusion at higher temperature and then extrapolated to lower temperatures. In addition, we believe that stress-strain phenomena captured in our atomistic systems are dependent mostly on bead-bead interactions, and not on entanglement. Therefore we are interested in matching the diffusion on the bead length scale and not on the polymer length scale. To match diffusion on this scale, we simulate a system of 500 molecules consisting of 3 monomers of polystyrene. The trimer contains all of the interaction components of a longer polymer chain, i.e., bond, angle, and nonbond. Figure 7 displays the dependence of the CG trimer diffusion with respect to dissipative scaling factor γ at 400 K. The nonbonded potential used in the CG simulation was parameterized using the FM method with the atomistic trimer diffusive trajectory at 400 K as input, while the IBI method was used to obtain the angle and bond potentials. We have fit an inverse power law to the data points to estimate the γ value at which the CG and atomistic diffusion coefficient match. This procedure was repeated at higher temperatures with the results presented in figure 8.

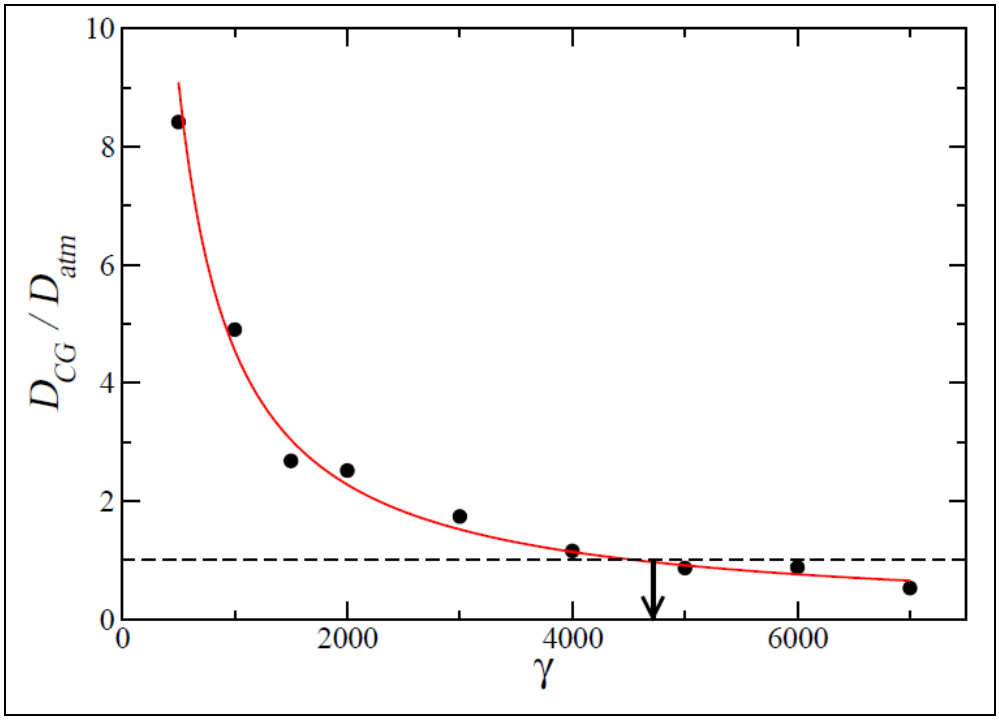

Figure 7. Relative diffusive speedup of the CG trimer system at 400 K as a function of the dissipative term γ. γ is in units of kcal /(mol fs). The symbols are simulation results, while the red curve is a fit to an inverse power law. An arrow indicates the value at which the CG and atomistic systems have the same diffusion.

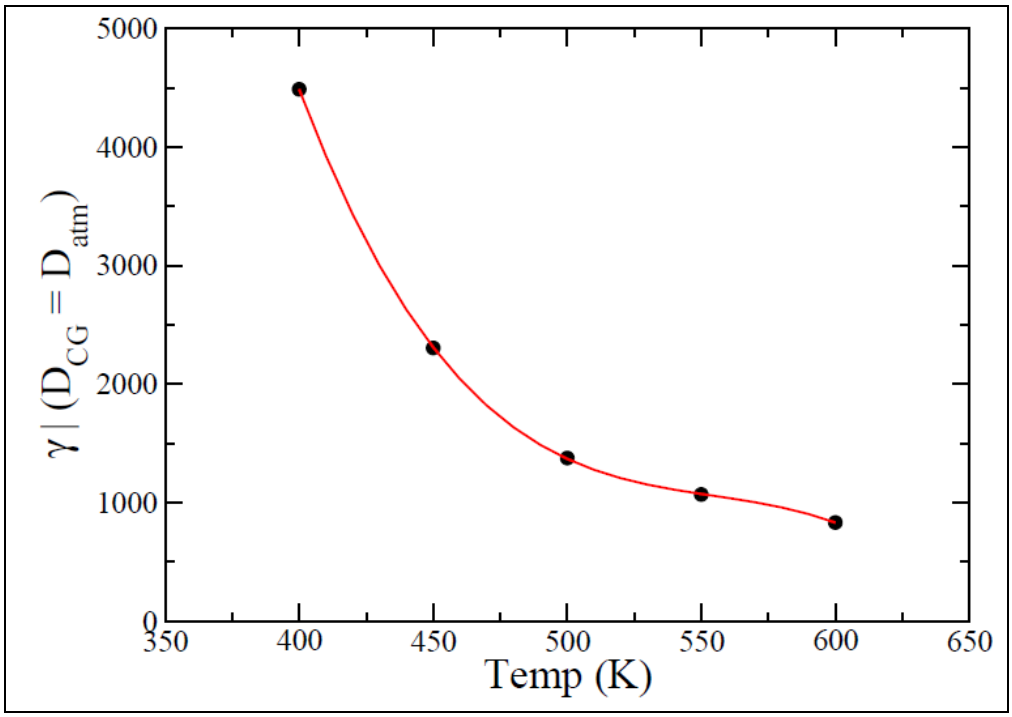

Figure 8. Dissipative term γ at which the diffusion of atomistic and CG systems are equal. The symbols are simulation results, while the red curve is a fit to a cubic polynomial.

A cubic polynomial was fit to the data and this equation was used to extrapolate to a value of γ = 45500 kcal/(mol fs) at 100 K. Performing stress-strain simulations with this dissipative term results in a curve presented in figure 9, which greatly improves the CG models's ability to match the stress-strain behavior compared to the atomistic system. The elastic modulus between the CG model determined using DPD and the atomistic model are now equal within statistical accuracy; however, the inelastic region does not match as well. Moreover, the CG system does not show any yield point and exhibits a strain hardening modulus that is larger than the atomistic system.

While figure 9 displays a systematic parameterization of a CG forcefield to describe mechanical properties, the potentials must have some transferability to other strain rates and temperatures to be practical. To probe the robustness of the parameters used in the DPD thermostat, we ran simulations at a slightly slower strain rate of 1e9 s^{-1} and 100 K, as well as the same strain rate and a higher temperature of 298 K, which are presented in figure 10. For the slightly slower strain rate, the dissipative term remained constant, while at 298 K γ = 8800 kcal/(mol fs). Strains were performed on only one replica; thus, the data in figure 10 is a little noisier than the other stress-strain curves.

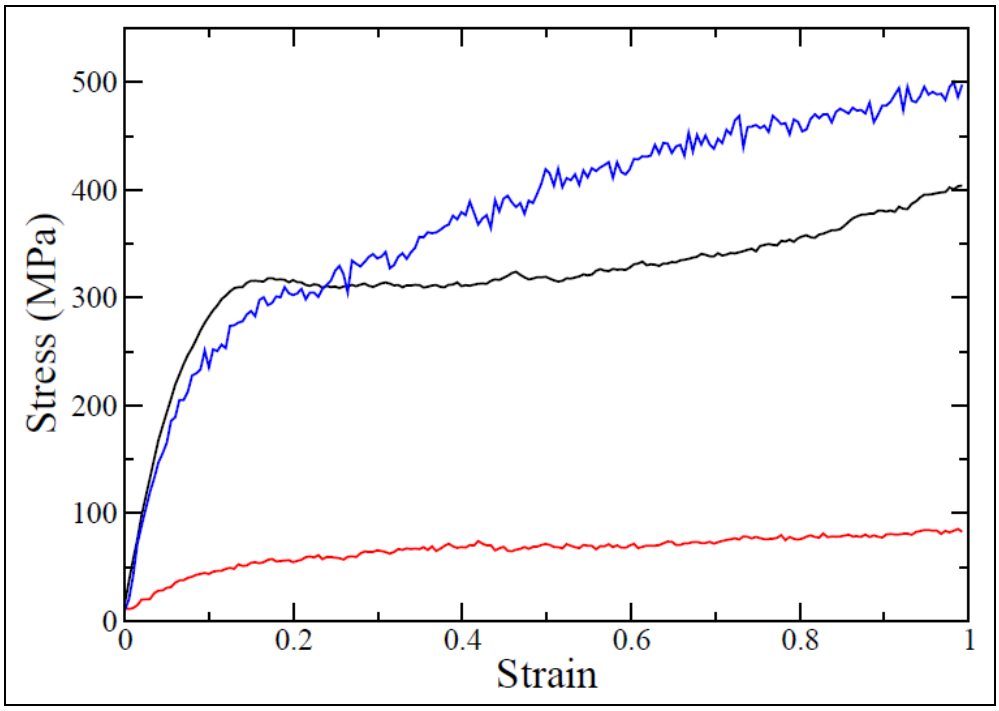

Figure 9. Stress-strain curves at 100 K and a strain rate of 5e9 s^{-1}. The black and red curves are the same as in figure 6, while the blue curve was generated using a DPD thermostat with a dissipative term γ = 45500 kcal/(mol fs).

For the slightly slower strain rate of 1e9 s^{-1}, the atomistic stress-strain behavior is essentially identical to the higher strain rate, yet the CG system displays marked differences between the two strain rates. At the slower strain rate, the CG system has a much lower elastic modulus and the behavior is almost rubbery in nature. The atomistic stress-strain curve at 298 K still appears glassy in nature with a smaller elastic modulus than at 100 K, as is expected. The CG stress-strain curve at the higher temperature is very similar to the higher strain rate-lower temperature curve, with no glassy characteristics. Overall, figure 10 suggests that the friction coefficient necessary to reconcile the CG and atomistic mechanical properties may be both temperature and strain-rate dependent.

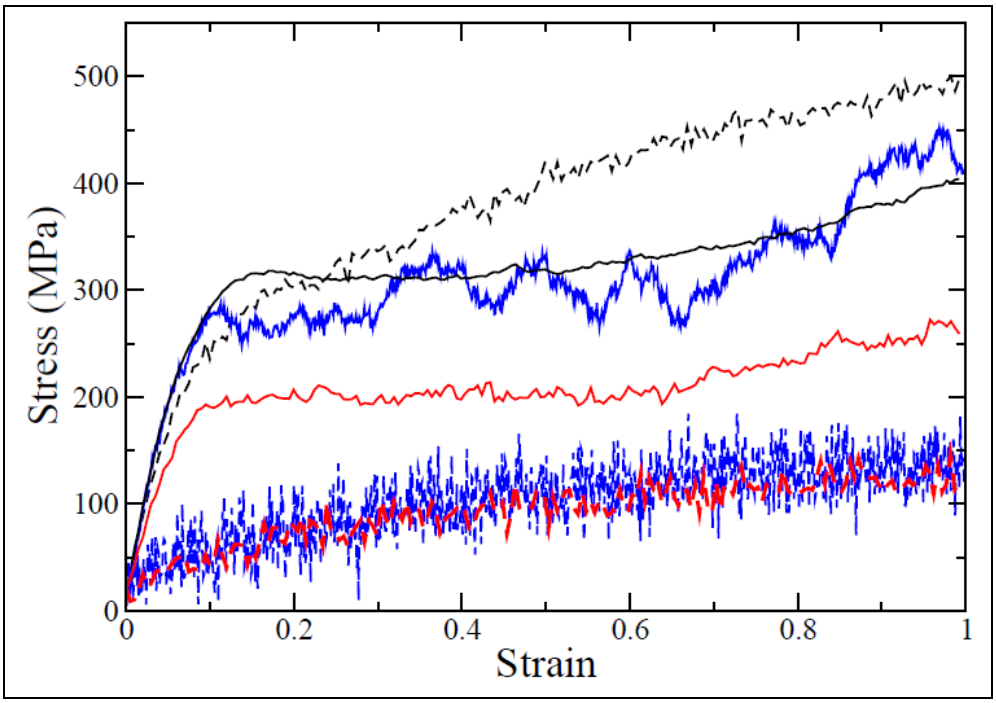

Figure 10. Stress-strain curves at two different strain rates and temperatures. Solid lines correspond to atomistic systems and dashed lines correspond to CG systems. Black curves are at a strain rate of 5e9 s^{-1} and 100 K (for CG system γ = 45500 kcal/(mol fs)). Blue curves are at a strain rate of 1e9 s^{-1} and 100 K (for CG system γ = 45500 kcal/(mol fs)). Red curves are at a strain rate of 5e9 s^{-1} and 298 K (for CG system γ = 8800 kcal/(mol fs)).

While adding dissipative forces to the system via the thermostat is not amenable to simple parameterization, an alternative is to directly alter the nonbonded interactions. Because the modulus of the CG system is much smaller than the atomistic system, it is apparent that the nonbonded potential needs to be more attractive to obtain a stiffer response. The simplest approach to induce more attraction is to uniformly shift the nonbonded forces to lower values. Following this approach, various constants were added to the nonbonded interaction and for each value the system was equilibrated at 500 K, quenched at 1 K/ps, and strained to 10% in the x-direction. For the value that demonstrated an elastic modulus closest to the atomistic model, the full stress-strain curve was generated in each direction. Figure 11 displays both the stress-strain curves corresponding to the system with the shifted nonbonded potential that matches the atomistic elastic modulus (red curve), as well a system with a slightly larger shift (blue curve). The shifted potential that matches the atomistic system contains a minimum of ~0.93 kcal/mol at 7.866 Å, down from ~0.53 kcal/mol at 8.1775 Å (see inset to figure 11). The overly stiff system corresponds to a potential containing a minimum of ~1.04 kcal/mol at 7.86 Å.

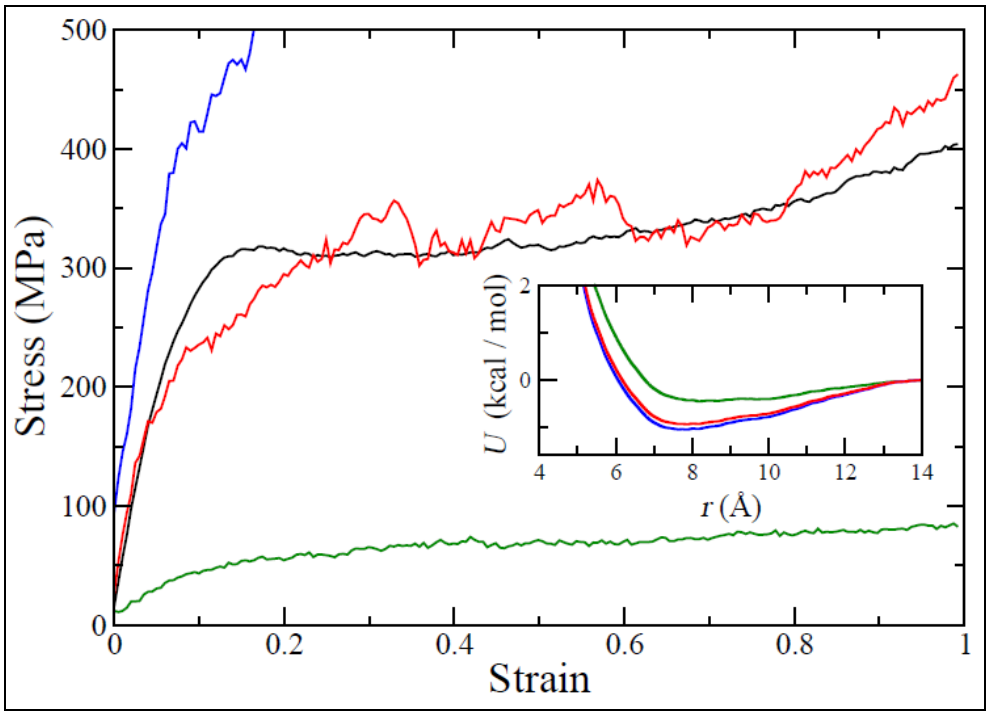

Figure 11. Stress-strain curves at 100 K and a strain rate of 5e9 s^{-1}. The black curve corresponds to the atomistic system. The green, red, and blue curves are for CG systems containing nonbonded interactions displayed in the inset. The green curve is the same as the lower curve in figure 9.

While the elastic region below 5% strain can be matched by a constant shift of the force, the CG potential is unable to reproduce the atomistic yield point, with a deviation occurring at a stress of ~200 MPa. In addition, the shifted potential significantly alters the structure of the CG system. Figure 12 displays the resulting bond, angle, and radial distributions upon equilibration at 500 K.

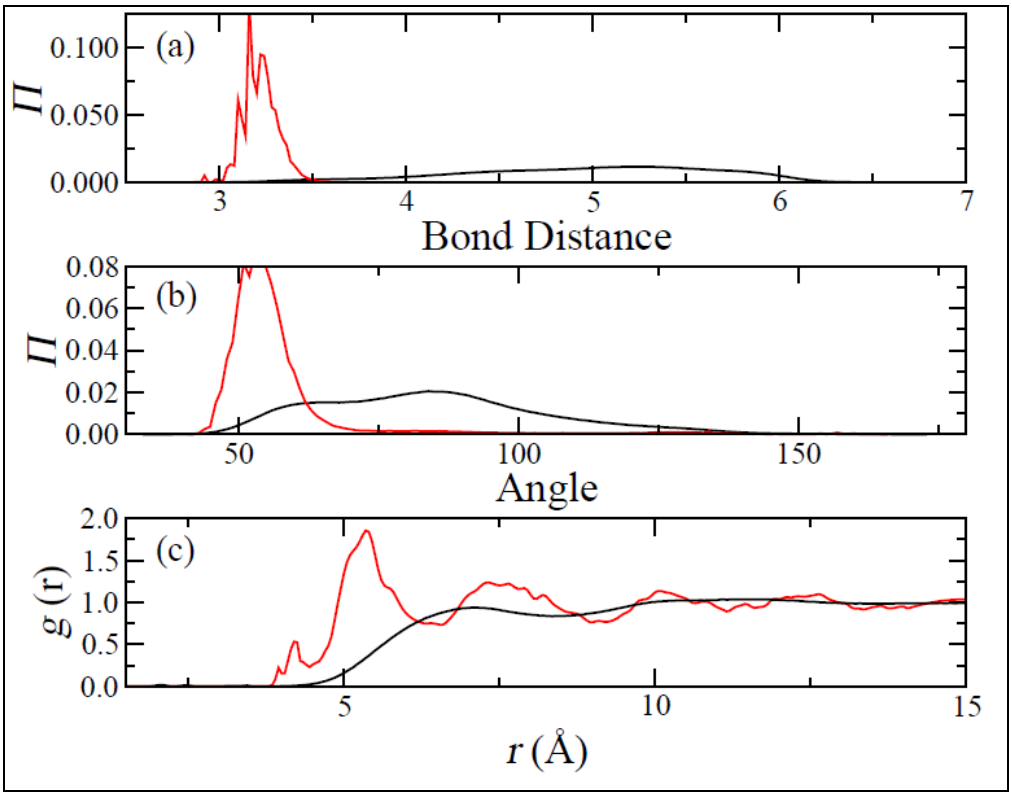

Figure 12. Distribution functions of the atomistic (black) and CG (red) models. (a), (b), and (c) are the bond, angle, and radial distribution functions.

The distributions in figure 12 demonstrate the destruction of the structure resulting from the increase in attraction between CG beads. The shifted nonbonded potential results in chains adopting smaller interbead separations, as well as more acute angular orientations. The radial distribution function also displays a much sharper peak at smaller separations as compared to the atomistic system.

While shifting the nonbonded potential to more attractive values has the desired effect on the mechanical properties, it has a decidedly undesired effect on the structure of the CG system. From the inset in figure 11, it is apparent that shifting the force by a constant amount influences the potential over the entire range of interactions. Alternatively, we attempted to lessen the destruction of the CG structure by shifting the force in only a small subset of the overall interaction range. We thus kept the location of the zero and minimum in the nonbonded potential constant by adding a sinusoidal function to the force

$$\begin{aligned} F_{new} &= F_{old} && r < r_0 \\ F_{new} &= F_{old} - A\sin\left(\pi * \left(\frac{r - r_0}{w}\right)\right) && r_0 \le r \le r_0 + w, \\ F_{new} &= F_{old} && r > r_0 + w \end{aligned} \tag{8}$$

where r_0 is the radius at which the nonbonded potential equals 0, A is the magnitude of the shift to the nonbonded potential, and w is twice the distance between the 0 and minimum in the nonbonded potential. The only adjustable parameter in the above equations is A, which controls the depth of the potential energy minimum, but not the location. Analogous to the procedure above, various values of A were chosen and the new potentials calculated. For each new potential, a CG system was equilibrated at 500 K for 2 ns, quenched to 100 K at 1 K/ps, and then strained to 10%. Figure 13 displays the full stress-strain curve corresponding to the choice of A that most satisfactorily matches the atomistic curve the best. The inset contains the nonbonded potential that corresponds to shifting the force with the sinusoidal function of equation 8. Compared to the potential obtained by shifting the force by a constant value, the sinusoidal shift localizes the increase in attraction to a much smaller range. The locally shifted potential results in a yield point and strain hardening modulus that more closely matches the atomistic system as compared to the uniformly shifted potential found in figure 11. Figure 14 displays the structural distribution functions associated with this locally shifted potential.

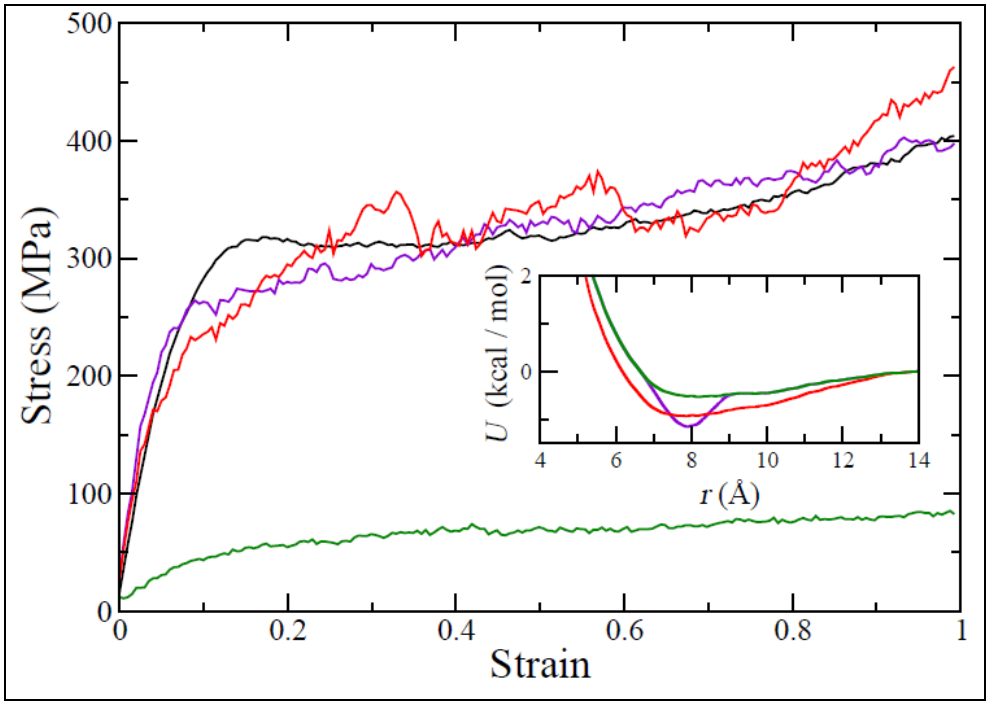

Figure 13. Stress-strain curves at 100 K and a strain rate of 5e9 s^{-1}. The black curve corresponds to the atomistic system. The green, red, and purple curves are for CG systems containing nonbonded interactions displayed in inset. The green and red curves are the same as the lower curve in figure 11.

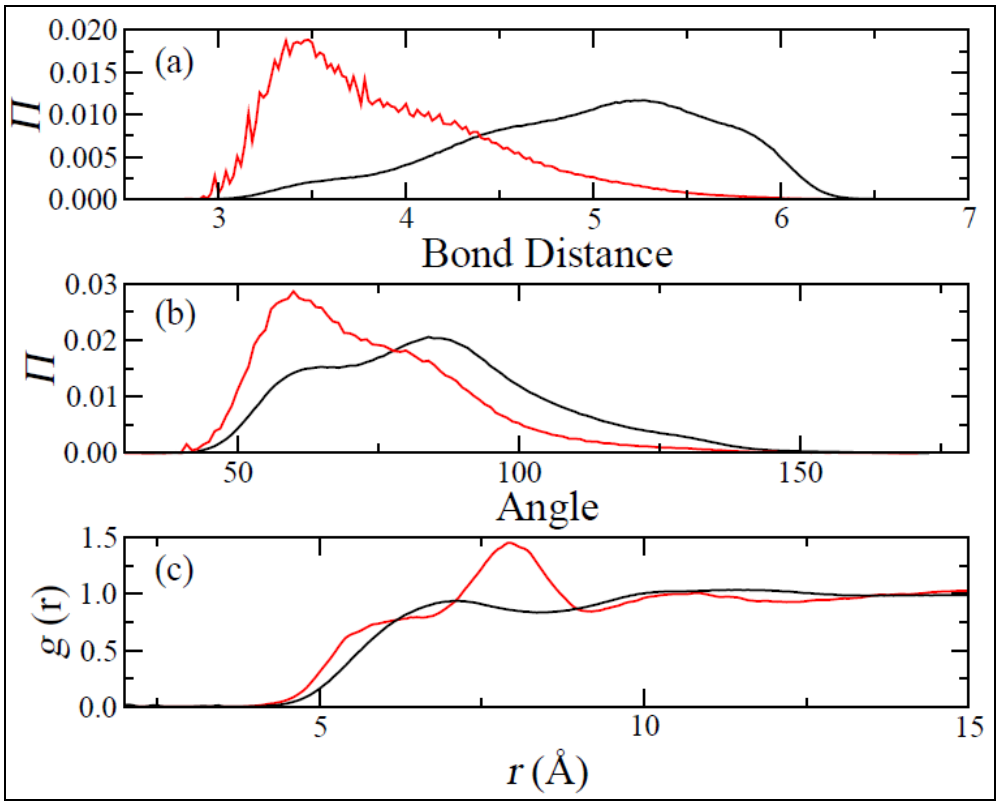

Figure 14. Distribution functions of the atomistic (black) and CG (red) models. (a), (b), and (c) are the bond, angle, and radial distribution functions.

While the locally shifted potentials produce structural distributions that deviate from the atomistic distributions, when compared to the uniformly shifted potentials, the deviation is not as significant. The CG bonded and angle distributions are shifted to lower values because of the added attraction, yet the radial distribution is affected only locally. A peak appears at slightly larger separations than the atomistic distribution. Overall, the protocol to add attraction to the CG model locally rather than uniformly results in slightly better stress-strain behavior and significantly better structural results.

The locally shifted potential was able to minimally impact equilibrium structural properties while matching mechanical properties at 100 K and a high strain rate, however, we also examined its applicability to other strain rates and temperatures. Figure 15 displays stress-strain curves at a slower strain rate of 1e8 s^{-1} and a temperature of 100 K. The locally shifted potential matches the atomistic behavior in the elastic region, yet yields at a slightly smaller value. In the elastic regime the locally shifted potential and atomistic systems display very similar behavior as well. The uniformly shifted potential yields at a much smaller value than the locally shifted CG system and atomistic system, and appears to have two distinct strain-hardening regions. From 0.05 to ~0.4 strain, the uniformly shifted potential has a region with a large strain hardening modulus, while strains larger than 0.4 produces a modulus very similar in value to the atomistic system. The fluctuations in the stress of the uniformly shifted potential are much larger in the elastic

region compared to the locally shifted potential system. Note that the CG stress-strain curves were generated using only one replica, thus it is not appropriate to compare the CG system fluctuations to the atomistic system.

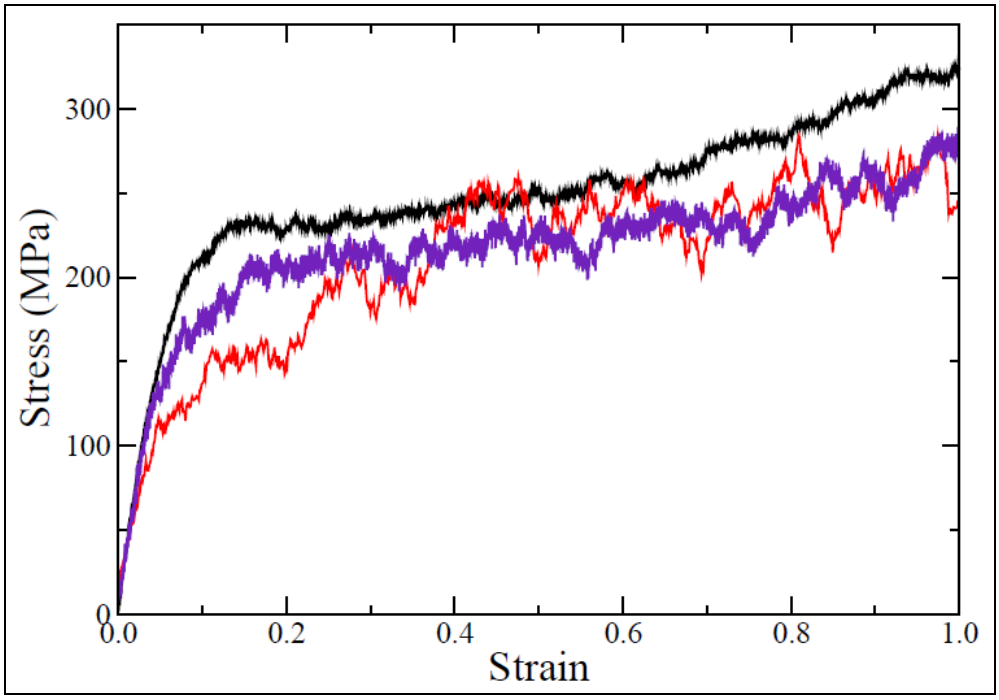

Figure 15. Stress-strain curves at 100 K and a strain rate of 1e8 s^{-1}. The black curve corresponds to the atomistic system. The red (uniformly shifted potential) and purple (locally shifted potential) curves are for CG systems containing nonbonded interactions displayed in the inset of figure 12.

Finally, we examined the transferability of the shifted potentials to describe stress-strain behavior at a different temperature. Figure 16 displays the stress-strain curves at 298 K and 5e9 s^{-1}. The locally shifted potential system has a smaller modulus and yield point compared to the atomistic system. While the elastic region of the locally shifted potential CG system does not match the atomistic system, the strain-hardening behavior does satisfactorily agree. The uniformly shifted potential transfers better to the higher temperature than the locally shifted potential, with both the elastic and inelastic region reasonably matching the atomistic model behavior.

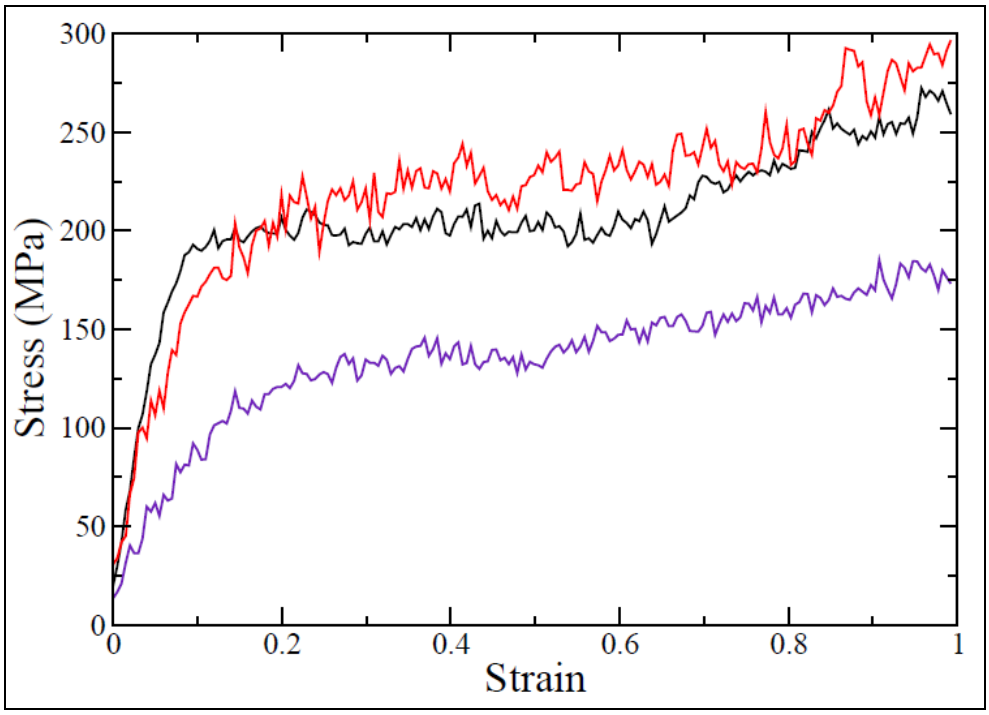

Figure 16. Stress-strain curves at 298 K and a strain rate of 5e9 s^{-1}. The black curve corresponds to the atomistic system. The red (uniformly shifted potential) and purple (locally shifted potential) curves are for CG systems containing nonbonded interactions displayed in the inset of figure 12.

4. Conclusion

We investigated the ability of a chemically informed CG potential of a single resolution (one monomer to one CG particle) to describe the mechanical behavior at glassy temperatures and high strain rate. The FM technique of Izvekov et al. was used to determine nonbonded interactions, while the IBI method was used to determine bonded and angular interactions. Applied in a straightforward manner, these techniques were insufficient to reproduce stress-strain behavior. Slowing down the dynamics of the CG system by implementing the constant temperature DPD method proved intractable. Matching the diffusion coefficients at higher temperatures by altering the DPD friction parameter γ gave satisfactory mechanical data at 100 K and a strain rate of 5e9 s^{-1}, yet did not transfer to different strain rates and temperatures. Two methods to introduce more attractive nonbonded interactions to the CG system were explored, a uniformly shifted force and a locally shifted force. The locally shifted force (which retained the potential's zero and minimum radial location) produced a better yield point as well as smaller fluctuations in the inelastic region as compared to the uniformly shifted force. In addition, the locally shifted potential has minimal impact on the equilibrium structure of the system. While transferability to different strain rates was reasonable, stress-strain behavior at higher

temperatures was poor compared to the uniformly shifted force. Future studies will examine a higher resolution CG model; two CG particles per one polymer monomer. The objective will be to determine the quantity (if any) that the potential needs to be altered to recover the atomistic models mechanical behavior. In addition, dihedral potentials will be added to this higher resolution and its effect will be explored.

5. References

1. Grest, G. S.; Kremer, K. Molecular-Dynamics Simulation for Polymers in the Presence of a Heat Bath. *Phys Rev A* **1986**, *33* (5), 3628–3631.

2. (a) Hoy, R. S.; Robbins, M. O. Strain hardening of polymer glasses: Effect of Entanglement Density, Temperature, and Rate. *J Polym Sci Pol Phys* **2006**, *44* (24), 3487–3500; (b) Hoy, R. S.; Robbins, M. O. Strain Hardening in Polymer Glasses: Limitations of Network Models. *Phys Rev Lett* **2007**, *99* (11); (c) Hoy, R. S.; Robbins, M. O. Strain Hardening of Polymer Glasses: Entanglements, Energetics, and Plasticity. *Phys Rev E* **2008**, *77* (3).

3. Bennemann, C.; Paul, W.; Binder, K.; Dunweg, B. Molecular-dynamics Simulations of the Thermal Glass Transition in Polymer Melts: Alpha-relaxation Behavior. *Phys Rev E* **1998**, *57* (1), 843–851.

4. Tsige, M.; Stevens, M. J. Effect of Cross-linker Functionality on the Adhesion of Highly Cross-linked Polymer Networks: A Molecular Dynamics Study of Epoxies. *Macromolecules* **2004**, *37* (2), 630–637.

5. Rottler, J.; Barsky, S.; Robbins, M. O. Cracks and Crazes: On Calculating the Macroscopic Fracture Energy of Glassy Polymers from Molecular Simulations. *Phys Rev Lett* **2002**, *89* (14).

6. Panico, M.; Narayanan, S.; Brinson, L. C. Simulations of Tensile Failure in Glassy Polymers: Effect of Cross-link Density. *Model Simul Mater Sc* **2010**, *18* (5).

7. Mukherji, D.; Abrams, C. F. Microvoid Formation and Strain Hardening in highly Cross-linked Polymer Networks. *Phys Rev E* **2008**, *78* (5).

8. Bulacu, M.; van der Giessen, E. Molecular-dynamics Simulation Study of the Glass Transition in Amorphous Polymers with Controlled Chain Stiffness. *Phys Rev E* **2007**, *76* (1).

9. (a) Lee, H. N.; Riggleman, R. A.; de Pablo, J. J.; Ediger, M. D. Deformation-Induced Mobility in Polymer Glasses During Multistep Creep Experiments and Simulations. *Macromolecules* **2009**, *42* (12), 4328–4336; (b) Riggleman, R. A.; Toepperwein, G. N.; Papakonstantopoulos, G. J.; de Pablo, J. J. Dynamics of a Glassy Polymer Nanocomposite during Active Deformation. *Macromolecules* **2009**, *42* (10), 3632–3640.

10. Reith, D.; Putz, M.; Muller-Plathe, F. Deriving Effective Mesoscale Potentials from Atomistic Simulations. *J Comput Chem* **2003**, *24* (13), 1624–1636.

11. (a) Carbone, P.; Varzaneh, H.A.K.; Chen, X. Y.; Muller-Plathe, F. Transferability of Coarse-grained Force Fields: The polymer Case. *J Chem Phys* **2008**, *128* (6); (b) Qian, H. J.; Carbone, P.; Chen, X. Y.; Karimi-Varzaneh, H. A.; Liew, C. C.; Muller-Plathet, F. Temperature-Transferable Coarse-Grained Potentials for Ethylbenzene, Polystyrene, and Their Mixtures. *Macromolecules* **2008**, *41* (24), 9919–9929.

12. Fritz, D.; Harmandaris, V. A.; Kremer, K.; van der Vegt, N.F.A. Coarse-Grained Polymer Melts Based on Isolated Atomistic Chains: Simulation of Polystyrene of Different Tacticities. *Macromolecules* **2009**, *42* (19), 7579–7588.

13. Guerrault, X.; Rousseau, B.; Farago, J. Dissipative Particle Dynamics Simulations of Polymer Melts. I. Building Potential of Mean Force for Polyethylene and Cis-polybutadiene. *J Chem Phys* **2004**, *121* (13), 6538–6546.

14. (a) Allen, E. C.; Rutledge, G. C. Evaluating the Transferability of Coarse-grained, Density-dependent Implicit Solvent Models to Mixtures and Chains. *J Chem Phys* **2009**, *130* (3); (b) Johnson, M. E.; Head-Gordon, T.; Louis, A. A. Representability Problems for Coarse-grained Water Potentials. *J Chem Phys* **2007**, *126* (14).

15. Izvekov, S.; Parrinello, M.; Burnham, C. J.; Voth, G. A. Effective Force Fields for Condensed Phase Systems from Ab Initio Molecular Dynamics Simulation: A New Method for Force-matching. *J Chem Phys* **2004**, *120* (23), 10896–10913.

16. Wang, Y. T.; Izvekov, S.; Yan, T. Y.; Voth, G. A. Multiscale Coarse-graining of Ionic Liquids. *J Phys Chem B* **2006**, *110* (8), 3564–3575.

17. Zhou, J.; Thorpe, I. F.; Izvekov, S.; Voth, G. A. Coarse-grained Peptide Modeling Using a Systematic Multiscale Approach. *Biophys J* **2007**, *92* (12), 4289–4303.

18. Izvekov, S.; Chung, P. W.; Rice, B. M. Particle-based Multiscale Coarse Graining with Density-dependent Potentials: Application to Molecular Crystals (hexahydro-1,3,5-trinitro-s-triazine). *J Chem Phys* **2011**, *135* (4).

19. Izvekov, S.; Chung, P. W.; Rice, B. M. The Multiscale Coarse-graining Method: Assessing its Accuracy and Introducing Density Dependent Coarse-grain Potentials. *J Chem Phys* **2010**, *133* (6).

20. (a) Lyulin, A. V.; Vorselaars, B.; Mazo, M. A.; Balabaev, N. K.; Michels, M.A.J. Strain Softening and Hardening of Amorphous Polymers: Atomistic Simulation of Bulk Mechanics and Local Dynamics. *Europhys Lett* **2005**, *71* (4), 618–624; (b) Vorselaars, B.; Lyulin, A. V.; Michels, M.A.J. Microscopic Mechanisms of Strain Hardening in Glassy Polymers. *Macromolecules* **2009**, *42* (15), 5829–5842.

21. Majumder, M. K.; Ramkumar, S.; Mahajan, D. K.; Basu, S. Coarse-graining Scheme for Simulating Uniaxial Stress-strain Response of Glassy Polymers Through Molecular Dynamics. *Phys Rev E* **2010**, *81* (1).

22. Sun, H.; Mumby, S. J.; Maple, J. R.; Hagler, A. T. An Ab-Initio Cff93 All-atom Force-field for Polycarbonates. *J Am Chem Soc* **1994**, *116* (7), 2978–2987.

23. Plimpton, S. Fast Parallel Algorithms for Short-Range Molecular-Dynamics. *J Comput Phys* **1995**, *117* (1), 1–19.

24. Izvekov, S.; Voth, G. A. A Multiscale Coarse-graining Method for Biomolecular Systems. *J Phys Chem B* **2005**, *109* (7), 2469–2473.

25. Vorselaars, B.; Lyulin, A. V.; Michels, M.A.J. Deforming Glassy Polystyrene: Influence of Pressure, Thermal History, and deformation Mode on Yielding and Hardening. *J Chem Phys* **2009**, *130* (7).

26. Depa, P.; Chen, C. X.; Maranas, J. K. Why Are Coarse-grained Force Fields Too Fast? A Look at Dynamics of Four Coarse-grained Polymers. *J Chem Phys* **2011**, *134* (1).

27. Espanol, P.; Warren, P. Statistical-mechanics of Dissipative Particle Dynamics. *Europhys Lett* **1995**, *30* (4), 191–196.

List of Symbols, Abbreviations, and Acronyms

CG	coarse-grained
COMPASS	Condensed-phase Optimized Molecular Potentials for Atomic Simulation Studies
DPD	dissipative particle dynamics
FENE	finitely extensible nonlinear elastic
FM	force-matching
IBI	iterative Boltzmann inversion
LAMMPS	Large-scale Atomic/Molecular Massively Parallel Simulator
MAPS	Materials Processes and Simulations
MS-CG	multiscale coarse-graining
NPT	Isothermal-Isobaric
NVE	microcanonical ensemble

1 (PDF only) DEFENSE TECHNICAL INFORMATION CTR
DTIC OCA
8725 JOHN J KINGMAN RD
STE 0944
FORT BELVOIR VA 22060-6218

1 DIRECTOR
US ARMY RESEARCH LAB
IMAL HRA
2800 POWDER MILL RD
ADELPHI MD 20783-1197

1 DIRECTOR
US ARMY RESEARCH LAB
RDRL CIO LL
2800 POWDER MILL RD
ADELPHI MD 20783-1197

1 DIRECTOR
US ARMY RESEARCH LAB
RDRL CIO LT
2800 POWDER MILL RD
ADELPHI MD 20783-1197

3 DIRECTOR
US ARMY RESEARCH LAB
RDRL-WMM-G T ROSCH
BLDG 4600
APG MD 21005

INTENTIONALLY LEFT BLANK.